applied sciences

MDPI

Article

Prediction of Northeast China Cold Vortex Paths Based on Multi-Generator with Integrated Multimodal Features

Yuanzhen Jiao * and Dongyang Wu

College of Information Science and Technology & Artificial Intelligence, Nanjing Forestry University, Nanjing 210037, China
* Correspondence: yzjiao@njfu.edu.cn

Abstract

The Northeast China Cold Vortex (NCCV) is a crucial local synoptic system influencing the weather and climate of Northeast China. However, the application of artificial intelligence techniques in NCCV prediction remains limited. Based on ERA5 reanalysis data from the European Centre for Medium-Range Weather Forecasts (ECMWF), this study constructs a 23-year multi-modal spatiotemporal sequence dataset of NCCV via an objective identification method, focusing on NCCV trajectory prediction. An improved generative adversarial network model is proposed, which adopts a multi-encoder architecture to extract spatiotemporal features of multi-modal NCCV data and introduces a multi-generator structure to address the insufficient prediction capability of a single generator. A selector module is added to enable the model to adaptively select the optimal generation path. Ablation experiments show that compared with single-trajectory data input, multi-modal data input in our model reduces the average prediction error by 67.96 km, representing a 34.0% improvement, and the 24-h prediction error improvement reaches 39.7%. Ultimately, the proposed model achieves superior prediction accuracy and stability in the NCCV trajectory prediction tasks at 6 h, 12 h, 18 h, and 24 h, with prediction distance errors reduced by 21.4%, 29.2%, 34.0%, and 37.0% compared to LSTM.

Keywords: northeast China cold vortex; GANs; trajectory prediction

1. Introduction

The Cut Off Low (COL), also known as a closed low or cold pool, refers to a closed low-pressure system that forms in the middle to upper troposphere, having detached from the westerly jet stream [1]. Chinese scholars refer to the persistent and quasi-stationary Cut Off Lows that occur near the northeastern region as the Northeast China Cold Vortex (NCCV). The Northeast China Cold Vortex is a significant weather system unique to Northeast China [2], which not only has a profound impact on the weather and climate of the northeastern region but also has substantial implications for the weather and climate of the eastern parts of China and even East Asia as a whole [3]. Extreme NCCV activities can trigger severe weather events such as heavy rainfall, low temperatures, or thunderstorms in Northeast and eastern China [4], leading to agricultural losses and even threats to life and property. Therefore, understanding the development patterns of the Northeast China Cold Vortex and improving its forecasting capabilities are of paramount importance in reducing the occurrence of related disasters.

The study of the Northeast China Cold Vortex (NCCV) encompasses multiple dimensions. Researchers have developed various techniques for identifying cold vortices,

Check for updates

Academic Editor: Ephraim Suhir

Received: 23 January 2026
Revised: 25 February 2026
Accepted: 26 February 2026
Published: 26 February 2026

Copyright: © 2026 by the authors. Licensee MDPI, Basel, Switzerland. This article is an open access article distributed under the terms and conditions of the Creative Commons Attribution (CC BY) license.

such as employing Multivariate Empirical Orthogonal Functions (MV-EOF) to analyze the 500 hPa height field and temperature field, thereby identifying the intensity (first mode) and position (second mode) of the cold vortex [5]. Additionally, objective algorithms have been designed that integrate NCEP reanalysis data with global precipitation measurement products to identify 164 instances of strong precipitation cold vortex (HPCV) events from 2001 to 2019 [6]. Further, utilizing k-means clustering, the paths of cold vortices in early summer (June) were classified into four categories based on parameters such as source and motion direction: the eastward movement type, southeast long-distance movement type, eastward stationary type, and southward movement type of East Siberia [7]. Research on the structural characteristics of the Northeast Cold Vortex includes a 2013 study focused on the rainfall cloud associated with the Northeast Cold Vortex in Jilin Province during June 2005, which observed microphysical characteristics such as overcooled cloud thickness and high concentrations of ice particles within specific temperature ranges [8].

Currently, the forecasting of the NCCV primarily relies on numerical forecasting systems. Chen et al. [9] simulated the NCCV in June 2010 using the WRF model, clarifying the dominant types of transport associated with stratosphere-troposphere exchange during its lifecycle, as well as the variations in mass flux across the tropopause and the characteristics of net material exchange. Danling Liu et al. [10] utilized the CAMS-CSM (Chinese Academy of Meteorological Sciences Climate System Model) and conducted retrospective experiments using two different resolutions of reanalysis data to evaluate the climate model's performance in forecasting weather systems, specifically for NCCV events and the associated Meiyu during the onset of the 2020 Meiyu season. The results indicated that both the medium- and high-resolution CAMS-CSM models were able to capture NCCV events, although there were certain discrepancies in intensity, duration, and location. Additionally, in the realm of radar data assimilation, Feifei Shen et al. [11] found that using U-wind/V-wind (UV) as momentum control variables in the WRF-3DVar system better reflected convective-scale observational characteristics compared to stream function and velocity potential (WMX), improving the dynamical field and moisture convergence, thereby enhancing the forecasting accuracy of strong convection in the context of the NCCV. Consequently, it is evident that current efforts in NCCV forecasting are primarily focused on the analysis and prediction of heavy precipitation induced by the cold vortex background, with a notable lack of direct research on forecasting the movement paths of the Northeast China Cold Vortex.

The activity path of the NCCV directly determines the regions it affects and the intensity of weather conditions in those areas. Therefore, forecasting the cold vortex path is fundamental to predicting cold vortex-related weather. As early as 1976, Liu Chengqi et al. [12] established a predictive equation for the movement path of cold vortices using a combination of meteorological and statistical methods to forecast the future movement direction of the cold vortex. However, this method was overly simplistic, only predicting the movement direction of the NCCV without providing specific locations. In 1994, Sun Li et al. [13] categorized the Northeast China Cold Vortex into three types—northern vortex, central vortex, and southern vortex—based on its position. In 2020, Fang Y et al. [7] further classified the Northeast Cold Vortex into four types using k-means clustering, based on six features related to position paths, including the vortex generation location and movement direction. While Sun Li et al. focused solely on the generation location of the Northeast Cold Vortex, Fang Y et al. expanded their analysis to consider the movement direction as well. It is evident that the aforementioned studies do not provide direct predictions of the movement path of the NCCV.

In recent years, machine learning has played a significant role in various fields, including precipitation forecasting [14], meteorological disaster prediction [15], and typhoon

forecasting [16]. de Sousa Araújo et al. [17] proposed a method based on Long Short-Term Memory (LSTM) neural networks to predict extreme rainfall events in southeastern Brazil. This model is capable of forecasting precipitation amounts over the next six hours, demonstrating the potential of constructing regional models for extreme rainfall prediction using reanalysis data from global models. Zheng et al. [18] introduced a hybrid model that integrates ICEEMDAN, DenseNet, LSTM, and cubic polynomials, successfully predicting stepwise landslide displacements and providing effective landslide early warnings through a warning system. Xu et al. [19] proposed a novel spatiotemporal deep learning model named AM-ConvGRU for typhoon track prediction, addressing the challenges of extracting improved nonlinear features from the complex high-dimensional 3D structure of typhoons and effectively merging appropriate 2D and 3D features to enhance predictive accuracy.

The Northeast Cold Vortex and typhoons both exhibit characteristics of closed-circulation low-pressure vortex systems [20,21], sharing certain similarities. While machine learning has been increasingly applied in the identification and various predictions related to typhoons, its application in similar contexts, such as the Northeast China Cold Vortex, remains in its infancy or even non-existent. The prediction of the Northeast China Cold Vortex primarily relies on Numerical Weather Prediction (NWP), which incurs substantial computational and human resource costs. Utilizing machine learning methods to process data related to the NCCV and make predictions could effectively reduce forecasting costs and enhance the accuracy of predictions.

The main contributions of this paper are as follows: 1. We created a dataset of Northeast Cold Vortex (NCCV) from 2001 to 2023 that includes trajectory data (Trj) and reanalysis data (Re). Based on this, we introduced auxiliary feature data (X_{af}) to construct a multimodal NCCV time series. 2. Multiple generators were employed to address the inadequate learning ability of a single generator. 3. A generator selector was introduced, allowing each generator to specifically learn the characteristics of certain types of NCCVs, rather than learning features from all NCCVs.

The structure of this paper is organized as follows: Section 2 introduces the fundamental components of the models discussed, including LSTM, GAN, and 3D U-Net. Section 3 primarily describes the process of creating the multimodal NCCV time series dataset. Section 4 focuses on the various modules of MGEN-CVP and their loss functions. Section 5 presents comparative and ablation experiments to demonstrate the advantages of the model and the effectiveness of the multimodal data and its individual modules. Section 6 primarily presents the model's performance on the test set and conducts an analysis and discussion of the results.

2. Related Work

2.1. LSTM

Long Short-Term Memory(LSTM) is a specialized type of recurrent neural network designed for handling and predicting sequence data, with a particular strength in capturing long-term dependencies. It was first proposed in [22], laying the theoretical foundation for addressing sequence modeling challenges. The detailed structure of LSTM is illustrated in Figure 1. The core structure of LSTM comprises four key components: the forget gate, input gate, cell state, and output gate. Specifically, the forget gate decides which information to discard from the cell state, while the input gate regulates the integration of new information. The cell state is updated under the joint influence of these two gates, and the output gate determines the cell's current output—its gating mechanism functional logic was further refined to enhance model performance in [23]. A pivotal advantage of LSTM's gating design is its ability to effectively mitigate the gradient vanishing and explosion problems that plague traditional RNNs when processing long sequences. This enables LSTM to

preserve gradient integrity during backpropagation and better capture long-term sequence dependencies, as verified in the original work and subsequently summarized and validated in review research [22,24].

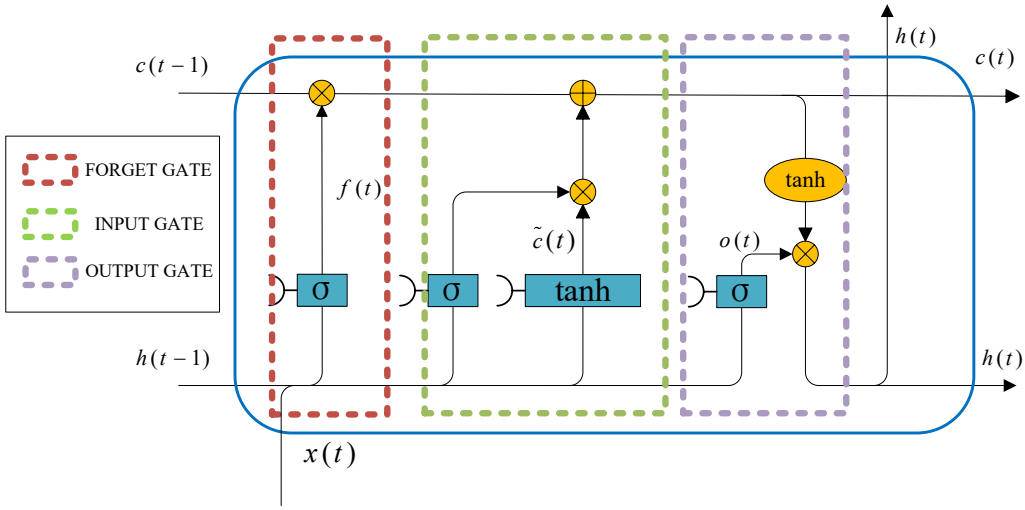

Figure 1. LSTM structure.

2.2. GAN

Generative Adversarial Network (GAN) is a type of deep learning model, structured as shown in Figure 2, primarily consisting of two components: the generator G and the discriminator D [25]. The generator G takes random noise $z \in \mathbb{R}^r$as input, aiming to generate data samples that appear realistic, thereby minimizing the generator loss $Loss_G$ to 'deceive' the discriminator. The generator loss function is as follows:

$$Loss_G = -E_{z \sim p_z(z)}[\log D(G(z))]$$

The discriminator D is responsible for determining whether the input samples are real (from the training dataset) or fake (from the generator). During the training process, the discriminator is iteratively trained using real samples and generated samples, with the goal of minimizing its classification error loss function, which is equivalent to maximizing the recognition rate for real samples and the misclassification probability for fake samples $Loss_D$:

$$Loss_D = -E_{x \sim p_{data}(x)}[logD(x)] - E_{z \sim p_z(z)}[log(1 - D(G(z)))]$$

At the same time, the generator optimizes the generated samples based on feedback from the discriminator, attempting to maximize the discriminator's classification errors on the generat ed samples. Ideally, training will reach a Nash equilibrium, at which point the discriminator cannot effectively distinguish between real samples and generated samples [26]. The overall optimization objective $L(G, D)$ is as follows:

$$\min_G \max_D L(D, G) = Loss_D + Loss_G$$

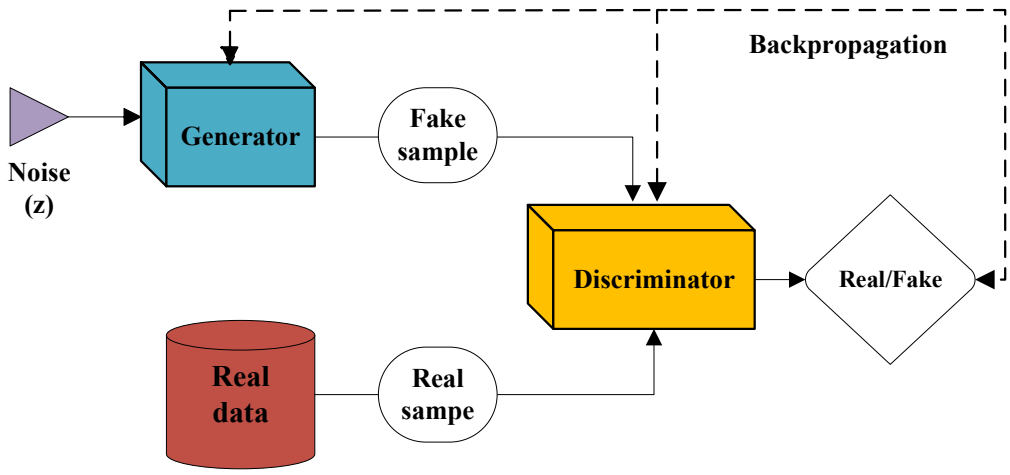

Figure 2. GAN structure.

2.3. 3D U-Net

U-Net is a convolutional neural network (CNN)-based architecture for image segmentation, originally designed for biomedical image segmentation tasks [27]. Its main feature is the use of a symmetric encoder-decoder structure, which combines downsampling and upsampling processes to effectively capture and reconstruct detailed information in images. 3D U-Net is an extension of U-Net, with a structure similar to 2D U-Net, but adjusted to handle volumetric data for three-dimensional inputs [28].

3D U-Net includes operations such as 3D convolution, upsampling, downsampling, and skip connections. The convolution operation is fundamental to 3D U-Net, and its formula is as follows:

$$Y(i,j,k) = \sum_{m=-\frac{K}{2}}^{\frac{K}{2}} \sum_{n=-\frac{K}{2}}^{\frac{K}{2}} \sum_{p=-\frac{K}{2}}^{\frac{K}{2}} X(i+m, j+n, k+p) \cdot W(m,n,p) + b$$

where: Y is the output feature map, X is the input feature map, W is the convolution kernel, b is the bias term, and pis the size of the convolution kernel. The max pooling operation is used for downsampling, and its formula is as follows:

$$Y(i,j,k) = \sum_{m=0}^{K-1} \sum_{n=0}^{K-1} \sum_{p=0}^{K-1} X\left(\frac{i}{s} - m, \frac{j}{s} - n, \frac{k}{s} - p\right) \cdot W(m,n,p)$$

Moreover, 3D U-Net utilizes skip connections to integrate features from the encoder with those from the decoder, thereby retaining spatial information and details.

3. Dataset Creation

This section introduces the data sources and specific construction procedures of the NCCV dataset employed in this study. The dataset consists of three components: the Northeast China Cold Vortex trajectory data (Trj), reanalysis gridded data (Re), and auxiliary data (X_{af}).

3.1. Raw Data

ERA5 is the fifth generation of global climate and weather reanalysis data launched by the European Centre for Medium-Range Weather Forecasts (ECMWF), covering meteorological records from 1940 to the present [29]. By combining global observational data with meteorological model data, ERA5 provides hourly meteorological estimates, including

atmospheric conditions, ocean wave data, and land surface parameters. In this paper, the reanalysis data of geopotential height (GPH), temperature (T), zonal wind component (U) and meridional wind component (V) at the 500 hPa pressure level, which were derived from ERA5 and recorded at 00:00, 06:00, 12:00 and 18:00 (UTC) daily during the period from 2001 to 2023, were selected as the data source for constructing the Northeast China Cold Vortex Database.

3.2. Identification and Tracking of NCCV

Definition 1. *A Northeast China Cold Vortex is a cyclonic system in the vicinity of northeast China that includes at least one closed contour line at the 500 hPa level, features a cold center, and persists for no less than 48 h.*

The objective identification and main characteristics of the Northeast Cold Vortex require consideration of multiple factors, including the height field, identification range, determination of the cold vortex center, temperature field, and cold vortex tracking. This paper references various methods for the identification and tracking of NCCV [3,30] and establishes the following criteria for their identification and tracking.

Cold vortex identification criteria:

- **Research domain:** Longitude 110° E to 145° E, Latitude 35° N to 60° N.
- **Low-pressure center:** In the 500 hPa geopotential height field, if a point is the lowest geopotential height within a 9 × 9 grid centered on that point (with a distance of 0.5° between each grid point), then this point is designated as the low-pressure center.
- **Cold center:** In the 500 hPa temperature field, if a point is the lowest temperature within a 9 × 9 grid centered on that point (with a distance of 0.5° between each grid point), then this point is designated as the cold center.
- **Cold vortex center:** 1. There must be at least one closed curve in the 500 hPa geopotential height field, with its center being the low-pressure center. 2. During the activity of the Northeast China Cold Vortex, the location of the low geopotential height center must correspond with a temperature low center (cold center) in the 500 hPa temperature field. 3. The wind direction north of the low-pressure center should be from the east, while the wind direction south of the low-pressure center should be from the west. If all three conditions are met, the location of the low-pressure center is designated as the cold vortex center, representing the overall position of the cold vortex.

The identification schematic of the cold vortex is shown in Figure 3.

Cold vortex tracking criteria: Within the designated study area, the low geopotential height center must persist continuously for 2 days or more. The continuously existing low center should not move more than 5° in the north-south and west directions every six hours, and should not move more than 10° to the east every six hours [30].

Furthermore, the algorithm presented in this study primarily focuses on the identification of closed isopleth systems and does not encompass the methodologies for identifying trough and ridge systems. Therefore, scenarios involving the temperature field without cold or warm centers, only featuring temperature troughs and ridges, are not considered.

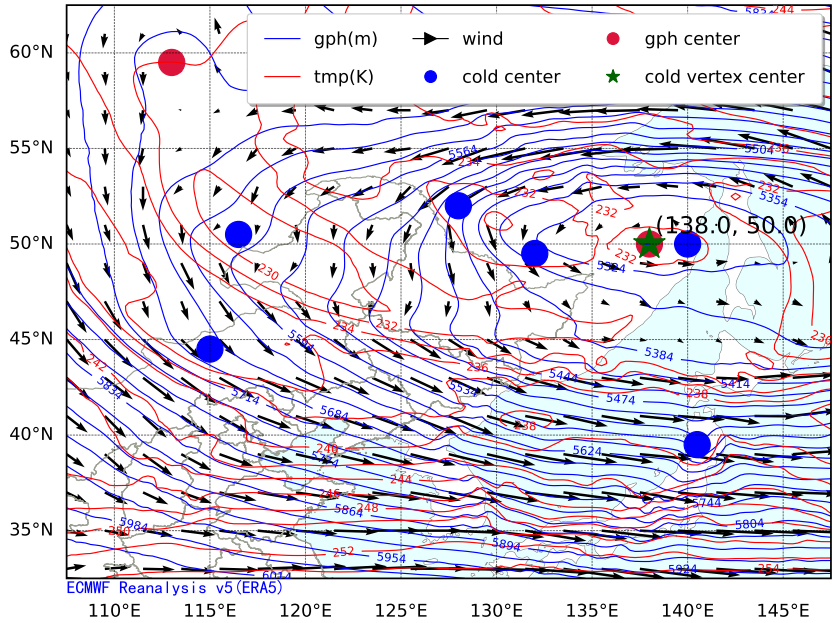

Figure 3. The identification schematic of the cold vortex.

3.3. Dataset Introduction

The NCCV dataset is derived from the aforementioned methodology and includes path data (including longitude and latitude sequences) for Northeast China's cold vortices from 2001 to 2023, as well as the reanalysis data for the geopotential height field at the 500 hPa level for corresponding times in the region. This dataset comprises a total of 1014 cold vortex events, each lasting at least 48 h, which collectively include 12,876 individual cold vortex instances. The specific contents of the dataset are shown in Table 1.

Table 1. NCCV dataset specific information.

Dataset	**NCCV**
Data type	NCCV track data and reanalyze data
Time span	2001–2023
Number of NCCVs	969
Latitude span	[35° N, 60° N]
Longitude span	[110° E, 145° E]
Time interval	6 h
Reanalyze data size (gph)	64 × 64

The NCCV dataset contains two different data modalities: Northeast cold vortex trajectory data and ERA5 reanalysis data. The NCCV trajectory data includes: a unique identifier for the cold vortex (ID), time (TIME), latitude (LAT), longitude (LON), cold vortex intensity (INT), and central wind speed (WND), where the cold vortex intensity also represents the geopotential height at the center of the cold vortex. For example, the trajectory data at four time points for the northeast cold vortex numbered 2001001 is shown in Table 2. The NCCV reanalysis data consists of a geopotential height (gph) matrix of size 64 × 64 near the center of the cold vortex.

Table 2. Trajectory data of northeast cold vortex No. 20010001: The times are from 00:00 on 2 January 2001 to 18:00 on 2 January 2001.

ID	Time	LAT (0.1° N)	LON (0.1° E)	INT (m)	WND (m/s)
20010001	2001010200	480	1380	5231	10.6
20010001	2001010206	480	1365	5216	7.3
20010001	2001010212	485	1320	5210	5.3
20010001	2001010218	490	1280	5191	4.2

3.4. NCCV Time Series

This section introduces the Northeast cold vortex time series samples used in this paper, along with their auxiliary features. The Northeast cold vortex time series samples X, which include auxiliary features, are as follows:

$$X = \{Trj, Re, X_{af}\}$$

$Trj = \{trj_1, trj_2, \ldots, trj_m\}$ is the time series of the northeast cold vortex's moving trajectory, and $Re = \{re_1, re_2, \ldots, re_m\}$ is the time series of the corresponding reanalysis data, where m is the number of time points included in the time series sample. $trj_t = [LAT_t, LON_t, INT_t, WND_t]$ and $re_t = matrix(gph_t)$ are t trajectory data and reanalysis data at time $t(t \in \{1, 2, \ldots, m\})$.

X_{af} is derived from the time series data $\{Trj, Re\}$ to enrich the features of the time series sample. X_{af} is extracted forward from the m-th time point as a reference, with the aim of maximizing the richness of the features at the m-th time point, which is the current moment. The features included are shown in Table 3.

Table 3. Description of X_{af}.

Feature Name	Remark
wind_class	magnitude of the central wind speed
month	current month
intensity_class	magnitude of the central intensity
move_volocity	movement speed of the most NCCV center
location_long	the longitude range of the NCCV center
location_lat	the latiitude range of the NCCV center
history_direction6	azimuth over the past 6 h
history_direction12	azimuth over the past 12 h
history_direction18	azimuth over the past 18 h
reanalyze_data0	reanalysis data at the m-th time point

4. Proposed Method

4.1. Problem Definition

This paper uses the Multi-GeneratorCold Vortex Prediction (MGEN-CVP) model to address the spatiotemporal prediction problem of predicting the moving trajectories of NCCV. The workflow of the entire model is as follows: Considering a specific cold vortex process in northeast China, suppose we have obtained cold vortex-related data at m time points. We need to predict the characteristics of the northeast cold vortex for the next n time points based on the data from the previous m time points. Thus, our model input is $X = \{Trj, Re, X_{af}\}$. When the model receives the input X, we hope it can output $\hat{Y} = \{\hat{y}_{m+1}, \hat{y}_{m+2}, \ldots, \hat{y}_{m+n}\}$ that closely approximates the true moving trajectory of the northeast cold vortex $Y = \{y_{m+1}, y_{m+2}, \ldots, y_{m+n}\}$, where $\widehat{y_t} = \left(\widehat{LAT^t}, \widehat{LONG^t}\right)$ and

$y_t = (LAT^t, LONG^t)$, with $t \in \{m+1, m+2, \ldots, m+n\}$ and n being the sequence length of the Northeast cold vortex to be predicted.

4.2. MGEN-CVP

MGEN-CVP is a prediction model based on Generative Adversarial Networks (GANs) that can accept data containing multiple dimensions and modalities. Therefore, we need to construct a corresponding network to handle different types of data, including an AF Net for processing auxiliary features and an encoder for extracting time series features of the NCCV. When we have sufficiently rich historical data of the NCCV and its auxiliary features, we use multiple generators to predict various potential movement trends of the NCCV. The model utilizes auxiliary features and historical trajectory information to select the generator that provides the most accurate predicted trajectory using a Generator Selector Network. In addition to the selector, a discriminator D is used to distinguish between real trajectories and predicted trajectories. Finally, we employ multiple loss functions to optimize MGEN-CVP to achieve the best performance. The overall structure of the network is shown in Figure 4. Next, we will sequentially introduce the feature extraction module, generator selection module, generator module, and discriminator module of the model.

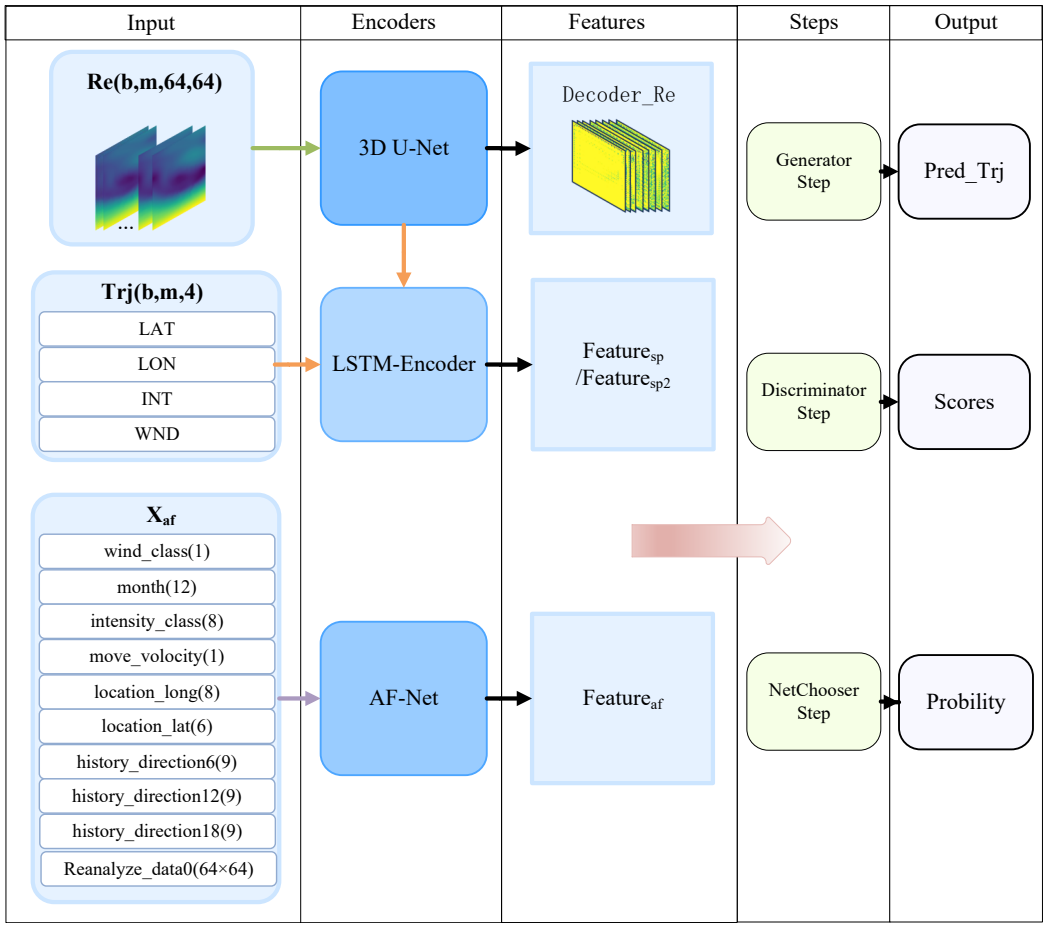

Figure 4. The overall structure of MGEN-CVP.

4.2.1. Feature Extraction Module

Since the model takes multimodal data as input, it is necessary to design different encoders for feature extraction from such data. As illustrated in Figure 4, the 3D-Unet, AF-Net, and LSTM-Encoder modules facilitate the extraction of features from the Northeast China Cold Vortex (NCCV) time-series data, which will be elaborated sequentially in the subsequent sections.

3D U-Net

We use a 3D U-Net network to extract spatiotemporal features from the Re data. The specific structure of our 3D U-Net is shown in Figure 5.

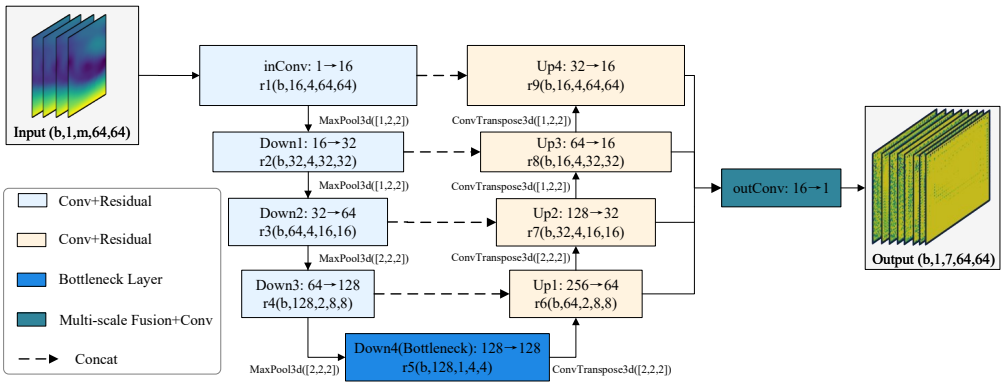

Figure 5. The structure of 3D U-Net.

As shown in Figure 5, the input to the U-Net is $Re \in \mathbb{R}^{b\times 1\times\times 64\times 64}$, where b is the batch size and $m = 4$. The tensor Reundergoes a series of convolutional and downsampling operations to extract features at different scales. Subsequently, the features are upsam pled and fused through skip connections, gradually restoring spatial resolution. Ultimately, an output feature is obtained through the multi-scale fusion module. The 3D U-Net consists of four downsampling steps, four upsampling steps, and the final multi-scale feature fusion, with the specific process detailed as follows:

$$
\begin{aligned}
r1 &= inConv(Re) \in \mathbb{R}^{b\times 16\times 4\times 64\times 64} \\
r2 &= down1(r1) \in \mathbb{R}^{b\times 32\times 4\times 32\times 32} \\
r3 &= down2(r2) \in \mathbb{R}^{b\times 64\times 4\times 16\times 16} \\
r4 &= down3(r3) \in \mathbb{R}^{b\times 128\times 2\times 8\times 8} \\
r5 &= down4(r4) \in \mathbb{R}^{b\times 128\times 1\times 4\times 4} \\
r6 &= up1(r5, r4) \in \mathbb{R}^{b\times 64\times 2\times 8\times 8} \\
r7 &= up2(r6, r3) \in \mathbb{R}^{b\times 32\times 4\times 16\times 16} \\
r8 &= up3(r7, r2) \in \mathbb{R}^{b\times 16\times 4\times 32\times 32} \\
r9 &= up4(r8, r1) \in \mathbb{R}^{b\times 16\times 4\times 64\times 64} \\
Unet_out &= outConv([r6, r7, r8, r9]) \in \mathbb{R}^{b\times 1\times 7\times 64\times 64}
\end{aligned}
$$

The Re data is a matrix sequence that can be considered as three-dimensional data; therefore, we use a 3D U-Net to capture its spatial features. Additionally, since Re is also a time series, the features obtained in Unet_out also contain temporal characteristics. Compared to Trj and X_{af}, Re has a higher dimensionality, thus we regard the feature Unet_out as highly significant.

AF-Net

We believe that the Northeast Cold Vortex information at the m-th time point has the greatest impact on the future movement trends of the Northeast Cold Vortex. Therefore, the model incorporates the features of X_{af} to assist the final selector in making more reliable choices. X_{af} includes one-dimensional (1D) features of varying lengths, as well as a two-dimensional (2D) data matrix gph. The AF-Net is capable of integrating features of different dimensions, and its specific structure is shown in Figure 6.

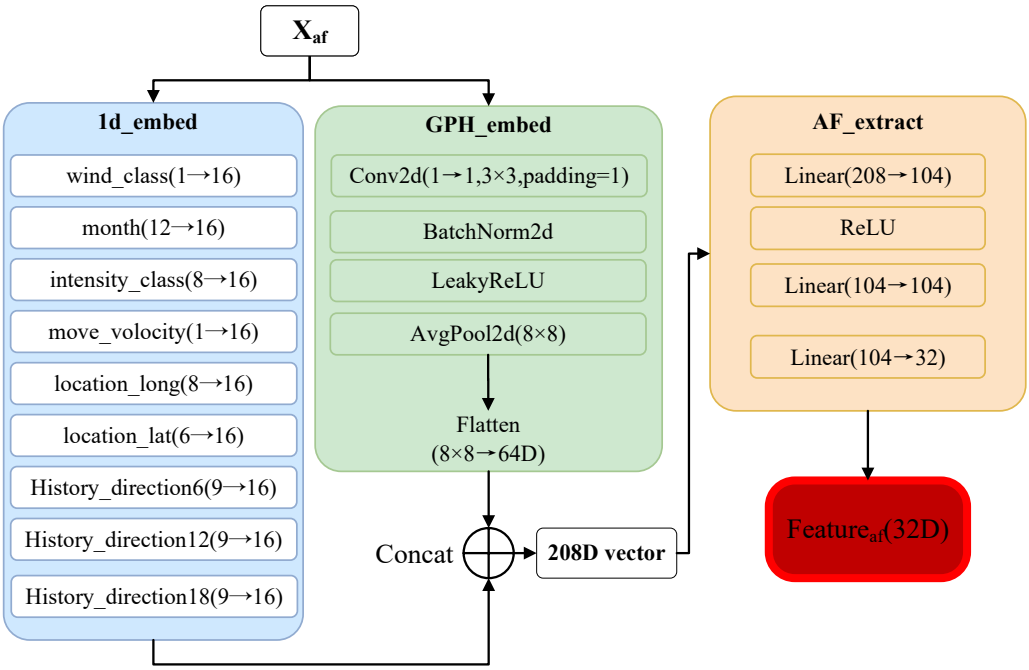

Figure 6. The structure of AF-Net.

AF-Net uses an MLP to process one-dimensional data. The gph data matrix can be regarded as an image, so we use a CNN to process gph and extract features. The two sets of features are concatenated to form a complete feature set, which is then passed through a multilayer perceptron to obtain the final auxiliary data feature $Feature_{af}$. The specific process is outlined as follows:

$$X^{i}_{1d_af} \in \mathbb{R}^{b\times 9\times len_i} (i \in \{1,2,\ldots,9\})$$
$$X_{2d_af} = matrix(gph) \in \mathbb{R}^{m\times 1\times 64\times 64}$$
$$E^{i}_{1d_af} = 1d_embed\left(X^{1d}_{af_i}\right) \in \mathbb{R}^{m\times 16} (i \in \{1,2,\ldots,9\})$$
$$E_{2d_af} = 2d_embed\left(X_{2d_af}\right) \in \mathbb{R}^{m\times 32}$$
$$E_{combined} = \left[E^{1}_{1d_af}, E^{2}_{1d_af}, \ldots, E^{9}_{1d_af}, E_{2d_af}\right]$$
$$Feature_{af} = MLP(E_{combined}) \in \mathbb{R}^{b\times 32}$$

LSTM-Encoder

The LSTM-Encoder is an LSTM-based network module that can extract spatiotemporal features from time series data. The trajectory prediction of the Northeast Cold Vortex can be viewed as a continuous medium path prediction problem in the meteorological field. LSTM is widely used in time series applications and has certain applications in spatiotemporal trajectory data prediction.

Since LSTM can effectively extract features that change over time in time series, we use it to capture the temporal changes in the Northeast Cold Vortex trajectory. The specific structure of the encoder is shown in Figure 7. The dimension of obs_{trj} is (m,b,4), where m is the length of the input sequence. Embed_Re is derived from Re through flattening and linear transformation. We unify both through an embedding layer to facilitate feature fusion.

Finally, the fused features are processed by the LSTM encoder to obtain spatiotemporal features. The entire process is outlined as follows:

$$E_{re} = Embed_{Re} \in \mathbb{R}^{m \times b \times 32}$$
$$Trj \in \mathbb{R}^{m \times b \times 4}$$
$$E_{Trj} = Linear(Trj) \in \mathbb{R}^{m \times b \times 32}$$
$$E_{combined1} = E_{re} + E_{trj} \in \mathbb{R}^{m \times b \times 32}$$
$$Feature_{sp} = LSTM(E_{combined1}, (h_0, c_0)) \in \mathbb{R}^{1 \times b \times 64}$$

where (h_0, c_0) represents the initial states of the hidden layer and cell layer.

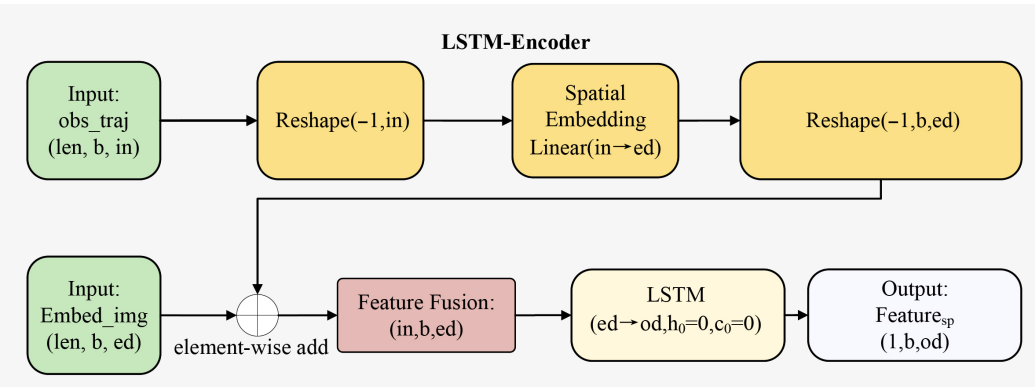

Figure 7. The structure of Encoder.

4.2.2. Generator Selector Network

The single-generator prediction method has the drawbacks of predicting out-of-distribution (OOD) samples and insufficient learning capability. We use a multi-generator approach to address these issues. We believe that in different northeast cold vortex predictions, the probability of selecting each generator varies, meaning that each generator may predict the trajectory of a specific type of northeast cold vortex more accurately. We hope our model can select the appropriate generator for prediction based on the historical spatiotemporal features $Feature_{sp}$ obtained from the northeast cold vortex time series $\{Trj,\ Re\}$ and the corresponding auxiliary features $Feature_{af}$. The selector first processes the features extracted from the time series and auxiliary data to create class distributions $P = softmax(logits) \in \mathbb{R}^{b \times num_gs}$, where num_gs is the number of generators. Then the output is the probability distribution for each selector being chosen $P = softmax(logits) \in \mathbb{R}^{b \times num_gs}$, which can also be represented as:

$$P_i = \begin{bmatrix} P_{i,1} \\ P_{i,2} \\ \vdots \\ P_{i,\text{num_gs}} \end{bmatrix} \quad (i \in \{1, 2, \ldots, b\})$$

Finally, the generator index sequence The generators with higher probabilities will be chosen more often, making their predictions for this type of northeast cold vortex more accurate.

The Generator Selector Network (GS-Net) determines the probability of each generator being selected based on the simple time series features of the northeast cold vortex, referred to as $Feature_{sp}$, and the features of auxiliary data that are more relevant to the m-th moment, denoted as $Feature_{af}$. It then conducts sampling based on this probability distribution to decide which generators to use for trajectory prediction. It serves two purposes: first, it

gives the probabilities of generator selection, which intuitively reflect each generator's capability to handle different types of northeast cold vortices; second, the generators with higher selection probabilities will have more opportunities to train on the cold vortex data in that specific situation, further enhancing their predictive ability for the trajectories of this type of northeast cold vortex. As mentioned above, using a single generator for predicting the trajectory of the northeast cold vortex has the disadvantage of insufficient learning capability. Therefore, we adopt a multi-generator approach for the prediction. These generators are homogeneous (of the same architecture) and can independently generate samples. With the use of a selector, each generator can train on different samples, allowing them to explore various generative spaces. Each generator will be more sensitive to specific types of northeast cold vortices, enabling more effective predictions for different trends of the northeast cold vortex. The structure of each generator is illustrated in Figure 8.

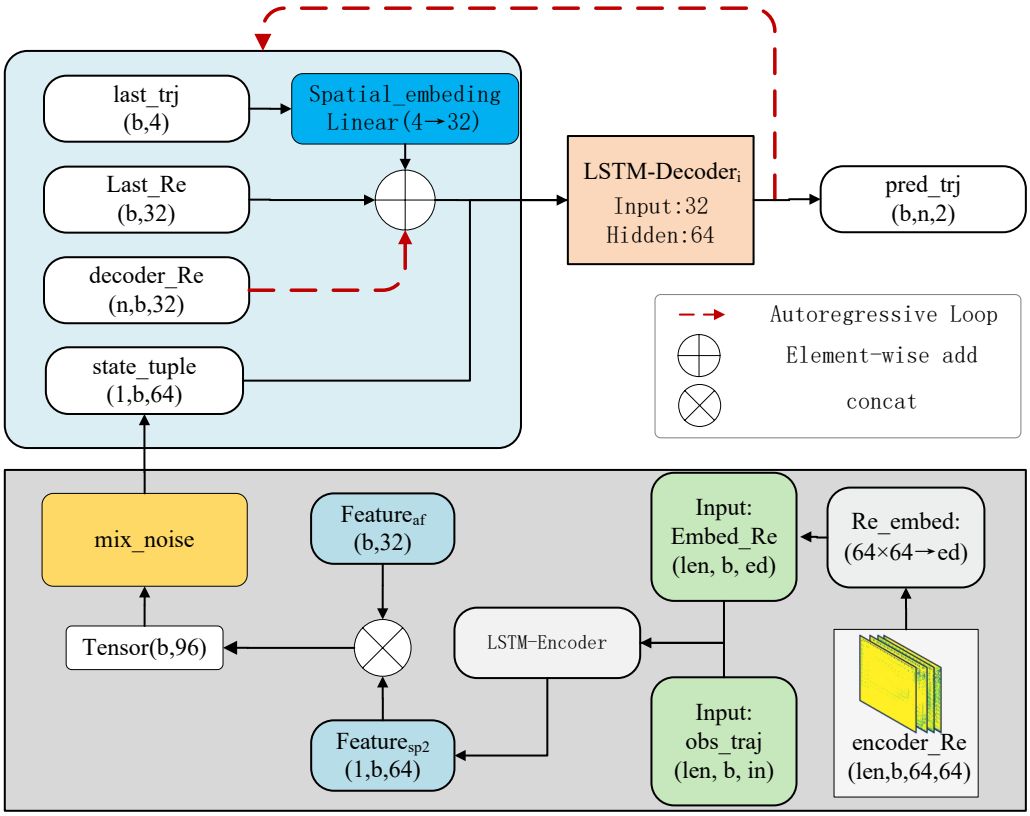

Figure 8. The structure of Generator.

The Multi-Generator contains multiple decoders, all of which share the same input. Therefore, the essence of using a selector to choose among the generators is, in fact, selecting between different decoders. The reason for this approach is that the output of the decoders is the predicted trajectory we ultimately need, while fixing the input to the decoders helps reduce the model's complexity and lowers the training costs.

In this step, the processing of the auxiliary data X_{af} related to the m-th moment remains unchanged; however, the feature extraction method for the time series $\{Trj,\ Re\}$ is more complex. In GS-Net, $Feature_{af}$ better reflects the state of the northeast cold vortex at the m-th moment, which is crucial for subsequent judgments about the movement trends of the cold vortex, making it a more important component. However, in the Multi-Generator, the extraction of features from the time series $\{Trj,\ Re\}$ becomes more significant, as it directly affects the accuracy of the final predictions made by the decoders. Therefore, it is necessary to employ more complex methods to extract richer spatiotemporal features.

In GS-Net, we simply flatten and embed Re, which neglects its more critical spatial features. Therefore, we use the Obs_Re data, reconstructed through the 3D U-Net, as the input for the encoder to obtain $Feature_{sp2} = LSTM - Encoder(Trj, encoder_{Re})$, which contains richer spatiotemporal features.

Each decoder is an LSTM-based decoder that receives the initial hidden state data (de_h_0, c_0) from the Mix_noise module, along with the trajectory of the cold vortex and the reanalysis data at the m-th moment. It ultimately produces the n-step prediction result $\hat{Y}$. The specific process is as follows:

$$(de_h_0, c_0) = Mix_noise(Feature_{sp2}, Feature_af)$$
$$\hat{Y} = LSTM - Decoder(trj_m, re_m, (de_h_0, w_0))$$

4.2.3. Discriminator

To ensure that the predictions of the generator closely align with the actual northeast cold vortex, we constructed a discriminator to extract features from the input data and determine whether the input data belongs to the real northeast cold vortex data $X_{real} = \{real_trj, real_re\}$ or the predicted northeast cold vortex data $X_{fake} = \{pred_trj, pred_re\}$. Taking the processing of X_{real} as an example, the structure of the discriminator is shown in Figure 9. The X_{real} data is encoded to extract features, and finally, a multi-layer perceptron outputs the discriminator's score for the input data. The entire process is as follows:

$$disEn_{in} = Encoder(real_trj, real_re)$$
$$scores = MLP(disEn_{in}) \in \mathbb{R}^{b \times 1}$$

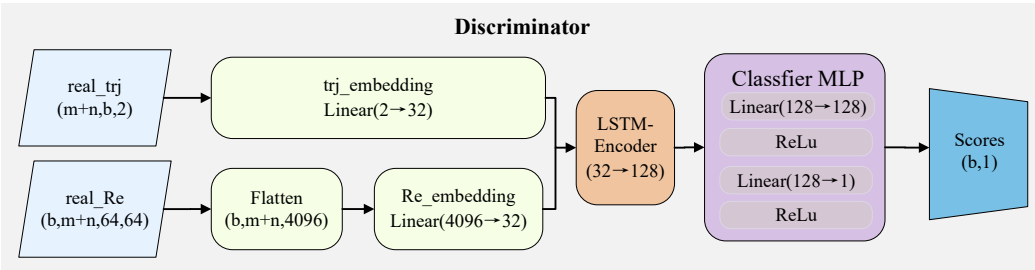

Figure 9. The structure of Generator.

In an ideal scenario, the discriminator can learn the patterns of NCCV development and regard any unreasonable trends as 'fake' during the training process.

4.3. Loss Functions

In the above, we introduced the feature extraction module, GS-Net, multi-generator module, and discriminator module in MGEN-CVP and analyzed their roles. We calculated several losses, including generator loss, discriminator loss, Re loss, optimal trajectory loss, and selector loss. These losses form three overall loss functions used to optimize the model: total generator loss, total discriminator loss, and selector loss.

4.3.1. Generator Step Loss

Generator loss: Our objective is to ensure that the data produced by generator G closely approximates the authentic northeast cold vortex data, while simultaneously guiding discriminator D to accurately classify this generated data as authentic The closer the

discriminator's judgment is to 1, the smaller the loss function value; conversely, the closer it is to 0, the larger the loss function value. The loss function for the generator is as follows:

$$\begin{aligned} L_G &= BCE(scores_{fake}, y_{fake}) \\ &= -\frac{1}{N}\sum_{i=1}^{N}(y^i_{fake} \cdot \log(\sigma(scores^i_{fake}))) \\ &\quad +(1-y^i_{fake}) \cdot \log(1-\sigma(scores^i_{fake})) \end{aligned}$$

Here, $BCE(.)$ represents the binary cross-entropy loss function, $\sigma(.)$ is the sigmoid function, and $y_{fake} = random.uniform(0.7, 1.0)$ is the target label value, which falls within the range (0.7, 1.0) rather than being a fixed value of 1. This approach, known as label smoothing, effectively prevents the generator from becoming overly confident and enhances the robustness of the model.

Re loss: We employed a 3D U-Net in the model to extract the spatiotemporal features of the northeast cold vortex reanalysis data. To better extract spatiotemporal features in *Re*, we added a reanalyze data loss to further optimize our 3D U-Net. This loss function primarily calculates the mean squared error between the actual reanalysis data Real_Re and the predicted reanalysis data *Pred_Re*, expressed as follows:

$$L_{Re} = \frac{1}{(m+1) \times 64 \times 64}\left\| Real_Re^{(m+n)} - Pred_Re^{(m+n)} \right\|_2^2$$

Here, $\|.\|_2^2$ represents the square of the L2 norm.

Minimun-of-N loss: MoN [31] serves as a metric in many multi-generator models; it calculates the minimum error among all results:

$$L_{MoN} = \min_{l} \|Y - \hat{Y}_i\|_2$$

Here, $i \in G_list$ and l represents the number of samples taken each time. The purpose of this loss is to encourage the generator to produce better predictions for the northeast cold vortex.

The total loss of the generator component is composed of the three parts mentioned above, with the primary objective of ensuring that the northeast cold vortex paths generated by the generator are closer to the real data. The total generator loss is as follows:

$$L_{G_total} = L_G + L_{re} + L_{MoN}$$

4.3.2. Discriminator Step Loss

Discriminator loss: The discriminator D is responsible for determining whether the input northeast cold vortex data is real. During the training process, the discriminator is iteratively trained using both real and generated samples, with the goal of minimizing its identification error loss function:

$$L_D = BCE(scores_{real}, y_{real}) + BCE\left(scores_{fake}, y_{fake}\right)$$

Here, label smoothing is also employed, where y_{real} is in the range of (0.7, 1.0) and y_{fake} is in the range of (0, 0.3). The total loss of the discriminator component consists of two parts: L_D and L_{Re}. The total loss function for the discriminator is as follows:

$$L_{D_total} = L_D + L_{Re}$$

4.3.3. Gnenrator Selector Step Loss

As mentioned earlier, GS-Net dynamically selects the appropriate generator (g) based on $Feature_{sp}$ and $Feature_{af}$ We designed the GS-Net loss function L_{GS} to enhance the selection capability of GS-Net. For convenience, we denote $Feature_{sp}$ as h_m and $Feature_{af}$ as f_{af}. The optimization process of this loss function is as follows:

First, we use the actual future trajectory coordinates (Y) and the predicted trajectory ($\hat{Y}$) from each candidate generator $g_i \in gid_list$ to assess the likelihood of generating the true trajectory under the current historical state h_m and auxiliary data features f_{af} . This is achieved through a Gaussian kernel-based likelihood function:

$$P\left(Y \mid h_m, f_{af}, g_i\right) \propto \frac{1}{l} \exp\left(\frac{-||\hat{Y}_i - Y||_2^2}{2\sigma}\right)$$

where l is the number of candidate generators. This likelihood value measures the closeness of the predictions $\hat{Y}_i$ from generator g_i to the true values Y (the smaller the L2 distance, the higher the likelihood).

Based on the likelihood values calculated in Step 1, we apply Bayes' rule to compute the posterior probability that each generator g_i is the ideal choice, given the known true future trajectory Y, historical state h_m, and auxiliary features f_{af}:

$$P(g_i \mid h_m, f_{af}, Y) = \frac{P(Y \mid h_m, f_{af}, g_i)}{\sum_{j=1}^{K} P(Y \mid h_m, f_{af}, g_j)}$$

This posterior probability distribution $P(g_i \mid h_m, f_{af}, Y)$ represents the likelihood of which generator is the optimal choice given the known 'answer' Y. It will serve as the target distribution for training GS-Net.

Finally, the GS-Net loss is defined as the cross-entropy between the target posterior probability distribution $P(g_i \mid h_m, f_{af}, Y)$ and the output distribution of GC-Net, $GS(h_m, f_{af})$:

$$L_{GS} = BCE\left(P(g_i \mid h_m, f_{af}, Y), GS(h_m, f_{af})\right)$$

Here, $GS(h_m, f_{af})$ is the probability distribution of the predicted generators based on the input from the GS-Net module (a probability array). By minimizing this cross-entropy loss L_{GS}, GS-Net is trained to learn to predict generator selection probabilities that are as consistent as possible with the 'optimal choice distribution given the known true answer Y in the current context (h_m, f_{af}).

5. Experiment

5.1. Experimental Setup

5.1.1. Dataset Partitioning

In the experiment, we set m = 4 and n = 4 to construct the NCCV time series, dividing it into three parts for training, validation, and testing. We selected 3386 samples from 2001 to 2019 as the training set, 411 samples from 2020 to 2021 as the validation set, and 328 samples from 2022 to 2023 as the testing set. The proportions of the training, validation, and testing sets account for 82%, 10%, and 8% of the total samples, respectively. The dataset partitioning adheres to the core principle of time series modeling—strict temporal order—using the most distant history for training, the closer history for validation, and the most recent for testing, thereby preventing data leakage and ensuring the fairness and reliability of model evaluation.

5.1.2. Dataset Preprocessing

Normalization is a mandatory step in modeling the northeast cold vortex time series. It lays the foundation for subsequent model predictions by eliminating dimensional differences, accelerating convergence, and enhancing model robustness. Particularly in the context of global climate change, normalization effectively separates long-term trends from short-term fluctuations, serving as a key technical guarantee for improving cold vortex prediction accuracy. We use the MAX_MIN method to normalize the northeast cold vortex trajectories and reanalysis data, with the following formula:

$$x' = \frac{x - min}{max - min}$$

5.1.3. Evaluation Metrics

We use Mean Absolute Error(MAE) and Root Mean Square Error(RMSE) as direct evaluation metrics for model predictions to assess the effectiveness of the model. The formulas for MAE and $RMSE$ are as follows:

$$MAE = \frac{1}{n}\sum_{i=1}^{n}\left|X_i - \hat{X}_i\right|$$

$$RMSE = \sqrt{\frac{1}{n}\sum_{i=1}^{n}\left(X_i - \hat{X}_i\right)^2}$$

To assess the model's prediction error for the position of the northeast cold vortex, we use the great-circle distance [32] to calculate the error distance between the true

$$Distance = 2 \times R \times \arcsin\left(\sqrt{\sin^2\left(\frac{|v_p - v_r|}{2}\right) + \cos v_p \cos v_r \sin^2\left(\frac{|u_p - u_r|}{2}\right)}\right)$$

where R is the radius of the Earth, v_r and u_r are the latitude and longitude of the actual northeast cold vortex, and v_p and u_p are the latitude and longitude of the northeast cold vortex predicted by the model.

5.2. Comparative Experiment

This experiment will compare the predictive performance of MGEN-CVP with several other algorithms, including LSTM [22], GRU [33], RNN [34], XGBoost [35], random forest [36], and transformer [37], to demonstrate the effectiveness of our model. The input for MGEN-CVP is the complete NCCV time series. Other algorithms cannot directly handle multimodal data, so their input consists of the *Trj* time series. The experimental results of MGEN-CVP using *Trj* as the sole input are provided in the ablation study section. We used data from four consecutive time points of the northeast cold vortex, representing 24 h of data, to predict the positions of the northeast cold vortex at the subsequent four consecutive time points. Our model first undergoes 5 rounds of pre-training, followed by 100 rounds of training, with num_gs set to 6. The other models are also trained for 100 rounds, with a batch size of 32.

Tables 4 and 5 summarize the Mean Absolute Error (MAE) and Root Mean Square Error (RMSE) metrics for various methods across different forecast lead times (6, 12, 18, and 24 h) in both latitude and longitude directions. As illustrated by the cumulative curves of MAE and RMSE in Figure 10, the MGEN-CVP model achieves the lowest cumulative errors in both directions. A closer examination of Tables 4 and 5 reveals that the MAE and RMSE for MGEN-CVP in the latitude direction are significantly lower than those of other

comparative methods. Moreover, it is observed that all methods exhibit generally higher errors in the longitude direction compared to the latitude direction, which may be associated with the movement characteristics of cold vortices. The NCCV demonstrates considerable movement in the east-west direction, while its movement in the north-south direction is relatively limited, potentially leading to the observed trend in the prediction results. Additionally, this phenomenon may be linked to the spatial measurement characteristics of geographic coordinates: the spacing between latitudes remains approximately constant, whereas the spacing between longitudes contracts with changes in latitude, thereby increasing the difficulty of predictions in the longitude direction.

Table 4. MAEs (0.1°) in latitude and longitude at times 6, 12, 18 and 24.

Methods	Latitude				Longitude			
	6 h	12 h	18 h	24 h	6 h	12 h	18 h	24 h
XGBoost	6.67	11.12	16.19	18.97	10.06	17.6	24.97	31.14
Random Forest	6.57	10.62	14.26	17.65	9.71	16.65	23.63	30.46
LSTM	6.05	9.22	12.67	15.87	9.2	14.92	20.74	26.69
GRU	6.13	9.25	12.56	15.75	9.46	14.97	20.85	27.05
RNN	6.51	9.29	12.56	15.69	9.64	15.35	20.68	26.67
Transformer	9.11	12.3	15.87	18.98	10.08	15.83	21.57	28.11
MGEN-CVP	**4.61**	**6.31**	**8.33**	**10.22**	**13.85**	**7.31**	**11.10**	**16.59**

Table 5. RSMEs (0.1°) in latitude and longitude at times 6, 12, 18 and 24.

Methods	Latitude				Longitude			
	6 h	12 h	18 h	24 h	6 h	12 h	18 h	24 h
XGBoost	8.6	14.2	20.79	23.95	13.7	22.96	30.84	39.3
Random Forest	8.57	13.5	18.41	22.88	13.24	22.28	30.39	37.91
LSTM	7.91	11.93	16.43	20.14	12.47	20.03	26.84	33.39
GRU	7.91	11.96	16.1	19.71	13.22	20.87	27.46	34.07
RNN	8.3	11.83	16.13	19.86	13.41	21.93	29.10	36.42
Transformer	11.25	15.35	20	23.82	13.76	21.37	28.19	33.33
MGEN-CVP	**6.02**	**8.22**	**10.60**	**13.03**	**10.02**	**14.24**	**17.68**	**20.73**

Specifically, in terms of the latitude MAE presented in Table 4, the MGEN-CVP method achieves values of 4.61, 6.31, 8.33, and 10.22 (in units of 0.1° N) for lead times of 6, 12, 18, and 24 h, respectively, representing relative reductions of approximately 24%, 32%, 34%, and 35% compared to the second-best method (which has values of approximately 6.05, 9.22, 12.56, and 15.69, also in units of 0.1° N). In the case of longitude MAE, MGEN-CVP shows values of 7.31, 11.10, 13.85, and 16.59 (in units of 0.1° E) for the same lead times, yielding relative reductions of approximately 21%, 26%, 33%, and 38% compared to the second-best method (approximately 9.20, 14.92, 20.68, and 26.67, also in units of 0.1° E).

Correspondingly, Table 5 indicates that the latitude RMSE values for MGEN-CVP are 6.02, 8.22, 10.60, and 13.03 (in units of 0.1° N) at lead times of 6, 12, 18, and 24 h, representing relative reductions of approximately 24%, 31%, 34%, and 34% compared to the second-best method (approximately 7.91, 11.93, 16.10, and 19.71, also in units of 0.1° N). For longitude RMSE, the values for MGEN-CVP are 10.02, 14.24, 17.68, and 20.73 (in units of 0.1° E), leading to relative reductions of approximately 20%, 29%, 34%, and 38% compared to the second-best method (approximately 12.47, 20.03, 26.84, and 33.39, also in units of 0.1° E).

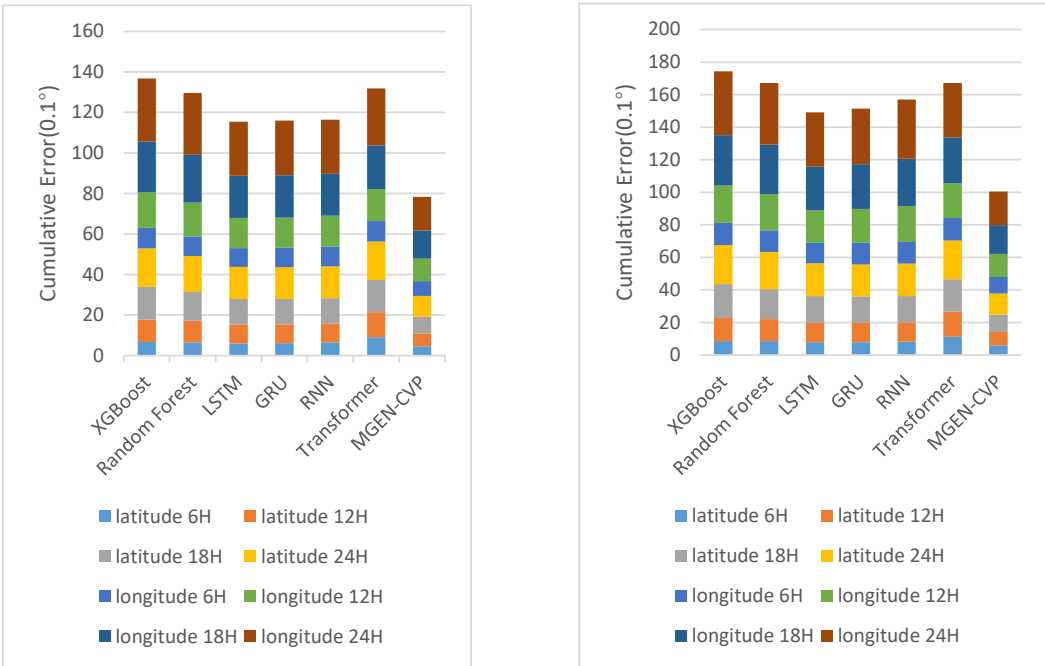

(**a**) MAE (**b**) RMSE

Figure 10. Stacking diagram of the MAE and RMSE for the longitude and latitudes prediction.

In the experiments, we utilized Distance as a metric to evaluate the final predictive performance of the models, with results presented in Table 6. From Table 6, it is evident that our MGEN-CVP method achieves the smallest prediction distance errors at each time point, significantly lower than those of other methods. Additionally, we found that the final predictive performance obtained using time series methods such as LSTM and GRU also outperforms that of tree-based methods like XGBoost.

Table 6. Distance (km) at times 6, 12, 18 and 24.

Methods	Time			
	6 h	**12 h**	**18 h**	**24 h**
XGBoost	112.96	195.08	280.1	340.94
Random Forest	135.57	196.7	258.48	320.4
LSTM	103.17	163.87	226.75	287.24
GRU	104.41	164.99	226.58	289.43
RNN	109.84	166.99	226.39	287.41
Transformer	135.57	196.7	258.48	320.4
MGEN-CVP	**81.05**	**115.96**	**149.61**	**181.07**

Specifically, the Distance metric reflects the spatial prediction bias of the models, with smaller values indicating more accurate trajectory position predictions. From a temporal perspective, the errors for all methods increase with the forecast horizon (from 6 h to 24 h), consistent with the principle that uncertainty accumulates over time. However, MGEN-CVP demonstrates a significantly reduced error growth rate at each time point, reflecting greater long-term predictive stability and generalization capability.

In a comparative analysis, MGEN-CVP shows substantial advantages over the best comparative methods at each prediction time point. At 6 h, compared to the second-best LSTM (103.17 km), MGEN-CVP achieves a Distance of 81.05, resulting in an absolute error reduction of 22.12 km, approximately a 21.4% relative decrease. At 12 h, compared to LSTM (163.87 km), the distance decreases to 115.96 km, with an absolute reduction of 47.91 km, or about a 29.2% relative decrease. At 18 h, compared to RNN (226.39 km), it drops to

149.61 km, with an absolute reduction of 76.78 km, approximately a 33.9% relative decrease. At 24 h, compared to LSTM (287.24 km), the distance decreases to 181.07 km, with an absolute reduction of 106.163 km, or about a 37.0% relative decrease.

It can also be observed that sequence modeling approaches like LSTM, GRU, and RNN generally outperform tree-based methods such as XGBoost and Random Forest. This indicates that explicit modeling of temporal dependencies is crucial for the medium- to long-term prediction of cold vortex trajectories. Furthermore, MGEN-CVP enhances this foundation by incorporating more effective spatiotemporal feature representations and prior fusion, allowing it to maintain lower biases and smoother error growth curves even in long-term predictions.

5.3. Ablation Analysis

In order to thoroughly assess the contributions of different data modalities to the predictive performance of the MGEN-CVP model for northeastern cold vortex trajectories, we designed four distinct data combinations for ablation experiments: **E1** utilizes only trajectory data (Trj), **E2** combines trajectory data with reanalysis data ($Trj + Re$), **E3** incorporates trajectory data along with auxiliary feature data ($Trj + Af$), and **E4** employs all three data modalities ($Trj + Re + Af$). The evaluation focuses on the contributions of different modalities to the final predictive performance, with the resulting prediction distance errors presented in Table 7.

Table 7. Data Ablation Experiment (km).

ID	Trj	Re	X_{af}	6 h	12 h	18 h	24 h	Average
E1	✓			97.38	167.94	233.72	300.49	199.88
E2	✓	✓		97.33	164.38	227.56	290.87	195.04
E3	✓		✓	95.24	145.82	196.33	251.67	172.27
E4	✓	✓	✓	**81.05**	**115.96**	**149.61**	**181.07**	**131.92**

The experimental results indicate that the introduction of reanalysis data significantly enhances the model's predictive performance. A comparison between E1 and E2 shows that the prediction errors at each time step decrease by 0.05 km, 3.56 km, 6.16 km, and 9.62 km, respectively, leading to an average error reduction from 199.88 km to 195.04 km, a decrease of 4.84 km. As the forecast horizon extends, the advantages of reanalysis data become increasingly apparent. In contrast, the contribution of auxiliary feature data is even more pronounced. A comparison between E1 and E3 reveals substantial reductions in prediction errors of 2.14 km, 22.12 km, 37.39 km, and 48.82 km at each time step, resulting in an average error decrease from 199.88 km to 172.27 km, a reduction of 27.61 km, demonstrating the excellent performance of auxiliary feature data in long-term predictions.

Furthermore, an analysis comparing E2 and E3 suggests that auxiliary feature data provide more effective spatiotemporal information than reanalysis data. The average error for E3 ($Trj + Af$) at 172.27 km is significantly lower than that for E2 ($Trj + Re$) at 195.04 km, with a difference of 22.77 km, indicating a greater contribution from the auxiliary feature data. A further comparison between E2 and E4 shows that incorporating auxiliary feature data on top of existing trajectory and reanalysis data yields substantial additional benefits, with errors decreasing by 16.28 km, 48.42 km, 77.95 km, and 109.80 km at each time step, resulting in an average error reduction from 195.04 km to 131.92 km, a decrease of 63.12 km. This highlights a clear synergistic effect between auxiliary feature data and reanalysis data.

Ultimately, the combination of all three data modalities in E4 achieves the best performance, with an average prediction error of 131.92 km, which is a reduction of 67.96 km compared to the baseline E1, representing an improvement of 34.0%. For long-term predictions

(24H), the error decreases from 300.49 km to 181.07 km, reflecting a 39.7% improvement. The results of the ablation experiments demonstrate the effectiveness of the multimodal design of the MGEN-CVP model, revealing significant synergistic effects between different data modalities. Combined usage outperforms individual modalities, and the advantages of multimodal data become more evident with extended prediction horizons. The comprehensive multimodal input significantly enhances the model's stability and accuracy across different time steps, validating the rationality of the model design and providing robust technical support for the prediction of northeastern cold vortex trajectories.

6. Analysis and Discussion

6.1. Analysis of Latitude and Longitude Prediction Error Distribution

Figure 11 illustrates the distribution characteristics of prediction errors for the NCCV trajectories over the next 24 h, as forecasted by the MGEN-CVP model on the test set. The figure employs a scatter plot format, with the true latitude and longitude values on the x-axis and the predicted latitude and longitude values on the y-axis. It systematically presents the prediction accuracy for different time scales (6 h, 12 h, 18 h, and 24 h) across eight subplots. Each subplot includes key evaluation metrics in the upper left corner: the correlation coefficient (R), Mean Absolute Error (MAE, in units of 0.1°), and Root Mean Square Error (RMSE, in units of 0.1°). The red dashed line in the figure represents the ideal prediction line (y = x); the closer the scatter points are to this line, the higher the prediction accuracy and stability.

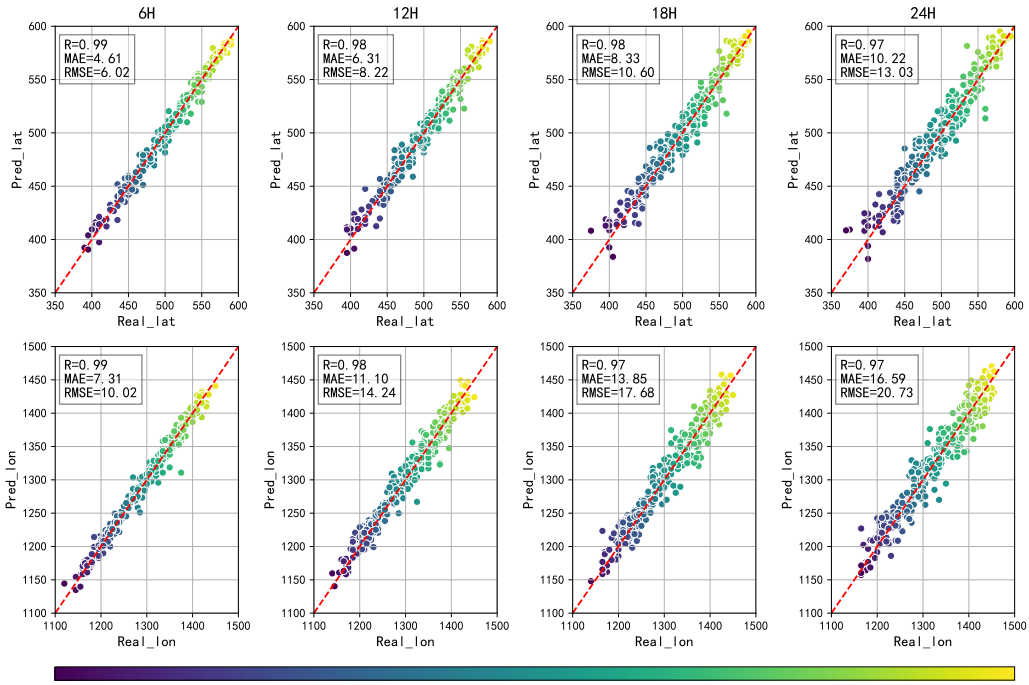

Figure 11. Latitude and longitude prediction error distribution.

The model demonstrates exceptional performance in latitude prediction, with correlation coefficients consistently exceeding 0.97 across all time scales. The highest prediction accuracy is observed at 6h (R = 0.99, MAE = 4.61, RMSE = 6.02), with scatter points densely clustered near the ideal line. As the forecast horizon extends, the errors gradually increase: at 12 h, the MAE rises to 6.31, and the RMSE is 8.22; at 18 h, the MAE reaches 8.33, with an RMSE of 10.60; and at 24 h, there is a significant increase in errors (MAE = 10.22, RMSE = 13.03), with the correlation coefficient dropping to 0.97. Longitude predictions similarly exhibit strong performance characteristics. The accuracy at 6h is outstanding

(R = 0.99, MAE = 7.31, RMSE = 10.02), with a highly concentrated scatter distribution. The 12h predictions maintain high accuracy (R = 0.98, MAE = 11.10, RMSE = 14.24). However, at 18 h, there is a noticeable increase in errors (R = 0.97, MAE = 13.85, RMSE = 17.68). At 24 h, the prediction errors significantly escalate (R = 0.97, MAE = 16.59, RMSE = 20.73), with the scatter distribution clearly deviating from the ideal line.

The model demonstrates excellent performance in predicting the latitude and longitude of northeastern cold vortices within an 18-hour timeframe, with all metrics showing a progressive increase as the forecast horizon extends. However, when the prediction time reaches 24 h, both MAE and RMSE for latitude and longitude predictions experience substantial increases, with the latitude correlation coefficient declining from 0.98 to 0.97. Overall, the model exhibits high accuracy and stability in trajectory predictions for 6 h, 12 h, and 18 h, but significant errors and reduced stability in the 24 h northeastern cold vortex position predictions reflect the amplification effect of cumulative errors in long-term forecasts.

6.2. Prediction Trajectory Analysis

This study presents the 24-h trajectory prediction results of various algorithms in the form of trajectory comparison plots, thereby better elucidating the advantages of our model (MGEN-CVP). Figure 12 displays the trajectory comparison for different algorithms concerning the cold vortex trajectory starting at 15 April 2022 12:00. The real trajectory includes the positions of the cold vortex at all eight time points, while the other predicted trajectories begin displaying the predicted points from the first prediction step. As illustrated in Figure 12, MGEN-CVP demonstrates greater accuracy in predicting the movement direction of northeastern cold vortices, a trend that is further confirmed in Figure 13. In Figure 13, the cold vortex trajectory exhibits two significant sharp angle changes, which MGEN-CVP effectively captures, providing reasonable trajectory predictions. In contrast, while the Transformer model also detects this trend, its predictions of movement distance are overly conservative, resulting in substantial deviations from the actual trajectory.

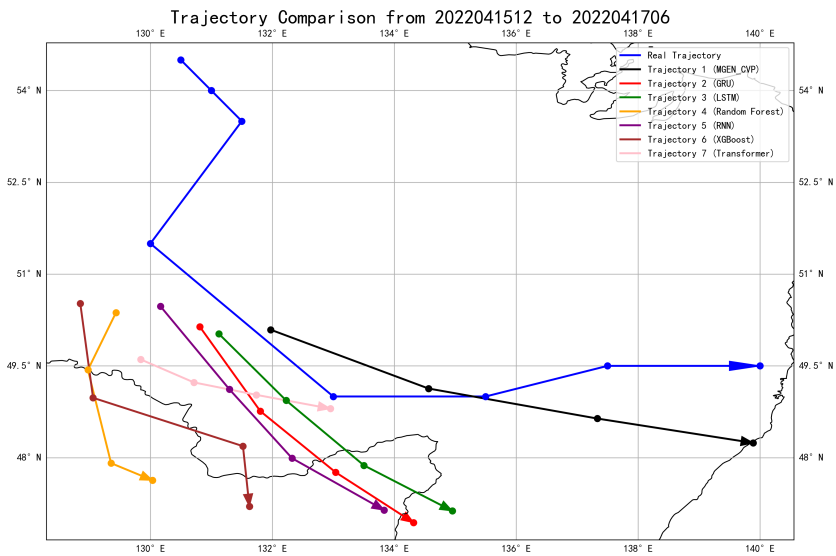

Figure 12. Trajectory Comparison from 20220410512 to 2022041716.

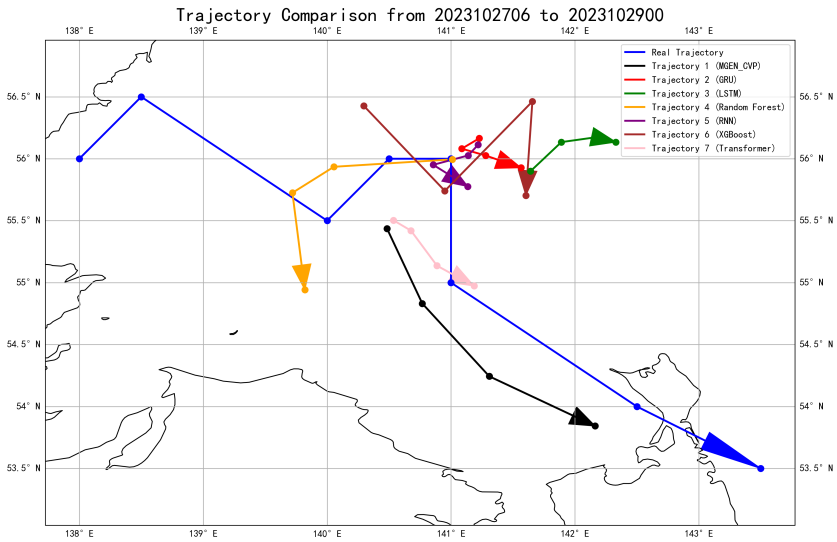

Figure 13. Trajectory Comparison from 2023102706 to 2023102900.

The true values of the trajectory of the NCCV in Figure 12 and the predicted values from different algorithms, along with the 24-h prediction distance error, are shown in Table 8. A quantitative analysis of the predictions from various models at 6 h, 12 h, 18 h, and 24 h time scales clearly reveals the significant advantages of the MGEN-CVP model in the cold vortex trajectory prediction task. Our model achieves superior performance in latitude prediction, especially for 24-h long-term forecasts. The predicted value is 48.2° N, with an error of only 1.3° relative to the observed value of 49.5° N. It outperforms most conventional machine learning approaches, while yielding a larger error compared with the Transformer model, which produces a prediction error of 0.7°. In comparison, XGBoost and Random Forest produced predicted values of 47.2° N and 47.6° N at 24 h, respectively, with deviations of 2.3° and 19°, demonstrating notable prediction drift.

Table 8. Prediction results of different models.

Model	Latitude (0.1° N)				Longitude (0.1° E)				Distance (km)
	6 h	12 h	18 h	24 h	6 h	12 h	18 h	24 h	24 h
realpath	490	490	495	495	1330	1355	1375	1400	0
XGBoost	505	490	482	472	1288	1291	1315	1316	670.89
Random Forest	504	494	479	476	1294	1290	1293	1300	765.13
LSTM	500	489	479	471	1311	1322	1335	1350	455.92
GRU	501	488	478	469	1308	1318	1330	1343	511.69
RNN	505	491	480	471	1302	1313	1323	1338	530.36
Transformer	496	492	490	488	1298	1307	1317	1330	514.83
MGEN-CVP	501	491	486	482	1319	1345	1373	1399	144.74

In longitude prediction, the MGEN-CVP model exhibits significantly superior performance. The 24-h predicted value is 139.9° E, which differs from the true value of 140.0° E by only 0.1°, corresponding to a prediction accuracy of 99.93%. This result is markedly superior to recurrent neural network models including LSTM (135.0° E, deviation 5.0°), GRU (134.3° E, deviation 5.7°), and RNN (133.8° E, deviation 6.2°), as well as the Transformer model (133.0° E, deviation 7.0°).

Furthermore, as shown in Figure 12, our model exhibits significantly better prediction stability over time scales compared to other algorithms. Throughout the prediction process from 6 h to 24 h, the prediction trajectory of our model is smoother and more continuous, avoiding the leaps and divergence in predicted values seen in other models during long-term predictions. In this sample's long-term prediction (24 h), although the latitude error of our model is greater than that of the Transformer model, the distance error is 144.74 km,

which is much lower than that of the Transformer model (514.83 km). Our model provides a more accurate prediction of the movement trajectory.

Traditional machine learning methods like XGBoost and Random Forest possess inherent limitations when processing time series data, making it challenging to effectively capture the spatiotemporal evolution characteristics of cold vortex trajectories, leading to significant declines in predictive accuracy over time. While LSTM, GRU, and RNN have advantages in sequence modeling, they still face issues of gradient vanishing and inadequate long-term dependency modeling when dealing with complex nonlinear spatiotemporal relationships. The MGEN-CVP model, through its generative adversarial network architecture, effectively combines the strengths of both the generator and discriminator, significantly enhancing the model's generalization capability and robustness while maintaining predictive accuracy. This model excels in learning the complex nonlinear patterns of cold vortex trajectories, thereby sustaining high predictive accuracy in long-term forecasting tasks.

6.3. Discussion

Our model has achieved a 24-h trajectory prediction for the Northeast China Cold Vortex, but there are several issues: The ERA5 data we used is not real-time, which means that MGEN-CVP cannot provide real-time trajectory forecasts for the Northeast cold vortex in practical applications.

Compared to the results of some typhoon prediction efforts, the trajectory prediction errors and actual distance errors of MGEN-CVP are relatively large. We believe the possible reasons are as follows: 1. The actual spatial resolution of the Northeast China Cold Vortex dataset self-developed in this paper is 0.5°, which is lower than that of commonly used typhoon datasets, and this will directly affect the accuracy of predictions. 2. The lifecycle of the Northeast cold vortex typically lasts 3–5 days, which prevents us from using longer historical data, such as 48-h time series, to predict future trajectory positions. Using longer historical data would reduce the sample size to a level that cannot support effective training.

7. Conclusions

This study leverages ERA5 data to develop the NCCV dataset and propose a multi-generator-based model that successfully forecasts northeastern cold vortex trajectories for the next 24 h. We enhance the spatiotemporal characteristics of NCCVs by employing multiple modalities of data, and the integration of multiple generators in conjunction with a selector enables each generator to deliver more precise predictions for specific types of cold vortex trajectories. Comparative and ablation experiments reveal that the utilization of multimodal data significantly augments predictive capabilities, leading to our model's superiority over other traditional methodologies.

Despite the successful implementation of trajectory predictions for NCCVs with the MGEN-CVP model, certain challenges and avenues for enhancement remain. Future endeavors and directions for refinement include: (1) establishing a higher-resolution NCCV dataset that can be accessed in real time; (2) refining the algorithm by incorporating reanalysis data beyond geopotential height (gph) to bolster the model's capacity to extract spatiotemporal features of northeastern cold vortices; (3) exploring the intensity of northeastern cold vortices and their associated precipitation forecasts, which will also constitute significant research avenues.

Author Contributions: Conceptualization, Y.J.; Methodology, Y.J. and D.W.; Software, Y.J.; Validation, Y.J. and D.W.; Formal analysis, Y.J.; Investigation, Y.J.; Resources, Y.J.; Data curation, Y.J.; Writing—original draft, Y.J.; Writing—review & editing, Y.J. and D.W.; Visualization, Y.J.; Supervision, D.W. All authors have read and agreed to the published version of the manuscript.

Funding: This research received no external funding.

Institutional Review Board Statement: Not applicable.

Informed Consent Statement: Not applicable.

Data Availability Statement: The data and code used in this study are publicly available in the GitHub repository: https://github.com/yuanzhenjiao123/MGEN-CVP, accessed on 10 February 2026.

Acknowledgments: The authors would like to thank the reviewers and editors of Applied Sciences for their valuable comments and suggestions, which have greatly improved the quality of this manuscript.

Conflicts of Interest: The authors declare no conflicts of interest.

References

1. Satoh, M. *Atmospheric Circulation Dynamics and General Circulation Models*; Springer Science & Business Media: Berlin/Heidelberg, Germany, 2013.
2. Liu, C.; Fang, Y.; Zhang, K.; Li, Y.; Wang, Y. Northeast China cold vortex is the key factor influencing the high-impact agroclimatic events in Northeast China. *Dyn. Atmos. Ocean.* **2024**, *107*, 101477. [CrossRef]
3. Sun, L. A study of the persistence activity of northeast cold vortex in China. *Sci. Atmos. Sin.* **1997**, *21*, 297–307.
4. Wu, J.; Liu, Y.; Li, Y.S.; Zuo, J.Q.; Nie, Y.; Li, Q.Q.; Wang, D.Q. The extreme Northeast China Cold Vortex activities in the late spring of 2021 and possible causes involved. *Adv. Clim. Chang. Res.* **2022**, *13*, 787–796. [CrossRef]
5. Xu, S.; Qi, L. Critical influence of the Northeast cold vortex in different positions on precipitation. *Clim. Dyn.* **2023**, *60*, 867–881. [CrossRef]
6. Chen, X.; Zhuge, X.; Zhang, X.; Wang, Y.; Xue, D. Objective identification and climatic characteristics of heavy-precipitation northeastern China cold vortexes. *Adv. Atmos. Sci.* **2023**, *40*, 305–316. [CrossRef]
7. Fang, Y.; Chen, H.; Lin, Y.; Zhao, C.; Lin, Y.; Zhou, F. Classification of Northeast China cold vortex activity paths in early summer based on k-means clustering and their climate impact. *Adv. Atmos. Sci.* **2021**, *38*, 400–412. [CrossRef]
8. Zhao, Z.; Lei, H. Observed microphysical structure of nimbostratus in northeast cold vortex over China. *Atmos. Res.* **2014**, *142*, 91–99. [CrossRef]
9. Chen, D.; Lü, D.; Chen, Z. Simulation of the stratosphere-troposphere exchange process in a typical cold vortex over Northeast China. *Sci. China Earth Sci.* **2014**, *57*, 1452–1463. [CrossRef]
10. Liu, D.; Wang, L. Evaluation of the CAMS-CSM Model in predicting a Northeast Cold Vortex Event at the early onset of 2020 Mei-yu season. *Atmos. Res.* **2022**, *280*, 106430. [CrossRef]
11. Shen, F.; Song, L.; Li, H.; He, Z.; Xu, D. Effects of different momentum control variables in radar data assimilation on the analysis and forecast of strong convective systems under the background of northeast cold vortex. *Atmos. Res.* **2022**, *280*, 106415. [CrossRef]
12. Liu, C.Q.; Li, G.C.; Chen, L.Y. Statistical forecast of the moving track of northeast cold vortex. *Chin. J. Atmos. Sci.* **1976**, 68–71. (In Chinese)
13. Sun, L.; Zheng, X.Y.; Wang, Q. The climatological characteristics of northeast cold vortex in China. *Quart. J. Appl. Meteor* **1994**, *5*, 297–303.
14. Su, Y.; Cheng, Q.; He, Y.; Liu, F.; Liu, J.; Zhu, J.; Rao, Y.; Chao, Y.; Liu, Z.; Chen, Y. An Evolution-Unet-ConvNeXt approach based on feature fusion for enhancing the accuracy of short-term precipitation forecasting. *Atmos. Res.* **2025**, *317*, 107984. [CrossRef]
15. Hao, Z.; Hao, F.; Singh, V.P. A general framework for multivariate multi-index drought prediction based on Multivariate Ensemble Streamflow Prediction (MESP). *J. Hydrol.* **2016**, *539*, 1–10. [CrossRef]
16. Jiang, W.; Zhang, D.; Hu, G.; Wu, T.; Liu, L.; Xiao, Y.; Duan, Z. Transformer-based tropical cyclone track and intensity forecasting. *J. Wind Eng. Ind. Aerodyn.* **2023**, *238*, 105440. [CrossRef]
17. de Sousa Araújo, A.; Silva, A.R.; Zárate, L.E. Extreme precipitation prediction based on neural network model–A case study for southeastern Brazil. *J. Hydrol.* **2022**, *606*, 127454. [CrossRef]
18. Zheng, Z.; Li, Y.; Zhang, Y.; Wen, L.; Kang, X.; Sun, X. Prediction and pre-warning of step-like landslide displacement based on deep learning coupled with ICEEMDAN. *Measurement* **2025**, *246*, 116585. [CrossRef]
19. Xu, G.; Xian, D.; Fournier-Viger, P.; Li, X.; Ye, Y.; Hu, X. AM-ConvGRU: A spatio-temporal model for typhoon path prediction. *Neural Comput. Appl.* **2022**, *34*, 5905–5921. [CrossRef]
20. Anthes, R. (Ed.) *Tropical Cyclones: Their Evolution, Structure and Effects*; Springer: Berlin/Heidelberg, Germany, 2016; Volume 19.
21. Xie, Z.; Bueh, C. Different types of cold vortex circulations over Northeast China and their weather impacts. *Mon. Weather Rev.* **2015**, *143*, 845–863. [CrossRef]

22. Hochreiter, S.; Schmidhuber, J. Long short-term memory. *Neural Comput.* **1997**, *9*, 1735–1780. [CrossRef]
23. Gers, F.A.; Schmidhuber, J.; Cummins, F. Learning to forget: Continual prediction with LSTM. *Neural Comput.* **2000**, *12*, 2451–2471. [CrossRef] [PubMed]
24. Greff, K.; Srivastava, R.K.; Koutník, J.; Steunebrink, B.R.; Schmidhuber, J. LSTM: A search space odyssey. *IEEE Trans. Neural Networks Learn. Syst.* **2017**, *28*, 2222–2232. [CrossRef]
25. Goodfellow, I.J.; Pouget-Abadie, J.; Mirza, M.; Xu, B.; Warde-Farley, D.; Ozair, S.; Courville, A.C.; Bengio, Y. Generative adversarial nets. *Adv. Neural Inf. Process. Syst. (NeurIPS)* **2014**, *27*, 2672–2680.
26. Goodfellow, I. NIPS 2016 tutorial: Generative adversarial networks. *arXiv* **2016**, arXiv:1701.00160.
27. Ronneberger, O.; Fischer, P.; Brox, T. U-net: Convolutional networks for biomedical image segmentation. In *International Conference on Medical Image Computing and Computer-Assisted Intervention*; Springer International Publishing: Cham, Switzerland, 2015; pp. 234–241.
28. Çiçek, Ö.; Abdulkadir, A.; Lienkamp, S.S.; Brox, T.; Ronneberger, O. 3D U-Net: Learning dense volumetric segmentation from sparse an notation. In *International Conference on Medical Image Computing and Computer-Assisted Intervention*; Springer International Publishing: Cham, Switzerland, 2016; pp. 424–432.
29. Hersbach, H.; Bell, B.; Berrisford, P.; Hirahara, S.; Horányi, A.; Muñoz-Sabater, J.; Thépaut, J.N. The ERA5 global reanalysis. *Q. J. R. Meteorol. Soc.* **2020**, *146*, 1999–2049. [CrossRef]
30. Huang, X.; Li, D. Objective identification method and variation characteristics of the Northeast China cold vortex from May to August of 1979–2018. *Acta Meteorol. Sin.* **2020**, *78*, 945–961.
31. Gupta, A.; Johnson, J.; Fei-Fei, L.; Savarese, S.; Alahi, A. Social GAN: Socially acceptable trajectories with generative adversarial networks. In *Proceedings of the IEEE Conference on Computer Vision and Pattern Recognition*; IEEE: Piscataway, NJ, USA, 2018; pp. 2255–2264.
32. Sinnott, R.W. Virtues of the Haversine. *Sky Telesc.* **1984**, *68*, 158.
33. Cho, K.; Van Merriënboer, B.; Gulcehre, C.; Bahdanau, D.; Bougares, F.; Schwenk, H.; Bengio, Y. Learning phrase representations using RNN encoder-decoder for statistical machine translation. *arXiv* **2014**, arXiv:1406.1078. [CrossRef]
34. Elman, J.L. Finding structure in time. *Cogn. Sci.* **1990**, *14*, 179–211. [CrossRef]
35. Chen, T. *XGBoost: A Scalable Tree Boosting System*; Cornell University: Ithaca, NY, USA, 2016.
36. Breiman, L. Random forests. *Mach. Learn.* **2001**, *45*, 5–32. [CrossRef]
37. Vaswani, A.; Shazeer, N.; Parmar, N.; Uszkoreit, J.; Jones, L.; Gomez, A.N.; Polosukhin, I. Attention is all you need. *Adv. Neural Inf. Process. Syst.* **2017**, *30*, 1–11.

Disclaimer/Publisher's Note: The statements, opinions and data contained in all publications are solely those of the individual author(s) and contributor(s) and not of MDPI and/or the editor(s). MDPI and/or the editor(s) disclaim responsibility for any injury to people or property resulting from any ideas, methods, instructions or products referred to in the content.